Journal of Solid State Chemistry **159,** 281–292 (2001)
doi:10.1006/jssc.2001.9157, available online at http://www.idealibrary.com on IDEAL®

A Comparative Structural and Magnetic Study of Three Compounds Based on the Cluster Unit $M_4Cl_8(THF)_6$ (M = Mn, Fe, Co)

H. Zhao,* R. Clérac,* J.-S. Sun,* X. Ouyang,* J. M. Clemente-Juan,† C. J. Gómez-García,† E. Coronado,† and K. R. Dunbar*,[1]

*Department of Chemistry, Texas A&M University, P.O. Box 30012, College Station, Texas 77842-3012; and †Instituto de Ciencia Molecular, Universidad de Valencia, 46100 Burjassot, Valencia, Spain
E-mail: dunbar@mail.chem.tamu

Received March 20, 2001; accepted March 21, 2001

IN DEDICATION TO THE LATE PROFESSOR OLIVIER KAHN FOR HIS PIONEERING CONTRIBUTIONS TO THE FIELD OF MOLECULAR MAGNETISM

Treatment of anhydrous MCl_2 phases with THF under refluxing conditions leads to excision of the clusters $M_4Cl_8(THF)_6$ (M = Fe (1), Co (3)) and dimensional reduction to the chain of clusters, $\{Mn_4Cl_8(THF)_6(Mn(THF)_2Cl_2\}_\infty$, (2). All three compounds were isolated in high yields as crystalline materials and subjected to comprehensive magnetic studies. X-ray structures of the three compounds were performed to verify the nature of the compounds, but only the Mn derivative is discussed in detail due to the fact that the structures of the Fe and Co clusters were reported earlier. The molecular structures of $M_4Cl_8(THF)_6$ (M = Fe, Co) consist of a rhombic arrrangement of metal ions with two octahedral and two pseudo-five-coordinate metal sites. The four outer edges of the cluster are each spanned by a chloride bridge, while the short diagonal is bridged by two chloride ions. The remainder of the coordination sites are occupied by two terminal chlorides and six THF solvent molecules. The 1D compound $\{Mn_4Cl_8(THF)_6(Mn(THF)_2Cl_2\}_\infty$, (2), is related to (1) and (3) in that the core of the structure is the same, but in this case the $M_4Cl_8(THF)_6$ units are linked by $MnCl_2(THF)_2$ bridges. The magnetic susceptibility data for $Fe_4Cl_8(THF)_6$ (1) and $Co_4Cl_8(THF)_6$ (3) in the high-temperature range are indicative of the presence of ferromagnetic and antiferromagnetic interactions respectively. Fitting of the data to anisotropic exchange models provided information on the intramolecular exchange parameters. In the low-temperature region, cooperative behavior was observed as a consequence of the presence of significant intercluster interactions. The Fe derivative behaves as a metamagnet, while the Co derivative is a weak ferromagnet below 3.5 K. In contrast to (1) and (3), the magnetic properties of $\{Mn_4Cl_8(THF)_6(Mn(THF)_2Cl_2\}_\infty$, (2), are indicative of the presence of antiferromagnetic exchange interactions within the cluster as well as between the neighboring clusters that lead to a nonmagnetic ground state. © 2001 Academic Press

[1]To whom correspondence should be addressed.

INTRODUCTION

One of the major themes of transition-metal coordination chemistry in the past 50 years has been the synthesis of clusters with diverse structures and interesting physical properties (1). Much of this chemistry is based on the reaction of polymeric materials with donor ligands that are capable of disrupting bridging interactions in the extended solid. The terms cluster excision (2) and dimensional reduction (3) have been used to refer to the process of removing a structural repeat unit of the solid, which is often a cluster M_xL_y. In principle, if one can isolate these "building blocks" from a cluster excision reaction, it becomes possible to "reconstruct" different solids based on new bridging groups. In this manner one can attempt to tailor the properties (e.g., magnetic, conducting, optical, etc.) and chemistry of the resulting materials.

The study of discrete, paramagnetic metal complexes has allowed chemists to build a foundation on which to base an understanding of the interactions between paramagnetic metal centers in larger assemblies (4). The use of paramagnets to systematically build clusters, chains, and higher dimensionality materials was pioneered by the later Olivier Kahn who often spoke of using these molecular "bricks" to build fascinating arrays and new magnetic materials (5). Research in our laboratories has also been inspired by the enormous opportunities for using molecules as building blocks for magnetic arrays (6, 7). One of our current interests is to isolate and characterize the magnetic behavior of 3D metal clusters that contain labile solvent molecules as part of their ligand environment. In considering candidates for this chemistry, we noted that a cluster excision process involving the reaction of $CoCl_2$ with tetrahydrofuran yields the tetranuclear species $Co_4X_8(THF)_6$ (8) whose molecular structure is related to the parent $CoCl_2$ material as indicated in Scheme 1. The two-dimensional layered material

0022-4596/01 $35.00

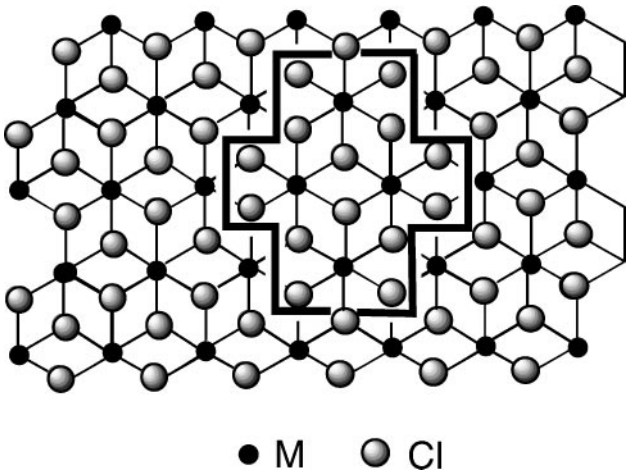

SCHEME 1. Portion of the CdI_2 layered structure, emphasizing the tetranuclear cluster fragment that is excised from the solid by THF.

is a common architecture for binary halides and is often referred to as the CdI_2-type framework. The related cluster $Fe_4X_8(THF)_6$ had earlier been reported from the reduction of $FeCl_3$ with Fe and with Cp_2ReH (9). We now report that the direct treatment of $FeCl_2$ and $MnCl_2$ with THF results in a cluster excision/dimensional reduction reaction to give high yields of $Fe_4X_8(THF)_6$ and the new 1D chain material $\{Mn_4Cl_8(THF)_6(Mn(THF)_2Cl_2\}_\infty$ respectively. A full treatment of the magnetic properties of the compounds was carried out. The behavior of the Fe and Co clusters is unusual, and contrasts with the magnetic behavior of the Mn chain compound. These new compounds may be viewed as soluble, reactive precursors of the paramagnetic materials MCl_2 (M = Mn, Fe, Co).

EXPERIMENTAL SECTION

A. General Methods

The starting materials, $FeCl_2$, $MnCl_2$, and $CoCl_2$ were purchased from Strem Chemicals, Inc., and used without further purification. The cluster $Co_4Cl_8(THF)_6$ was prepared according to the literature route (3). Acetone was distilled over 3-Å molecular sieves. Diethyl ether, hexanes, and THF were distilled over sodium-potassium/benzophenone, whereas methanol was distilled over $Mg(OMe)_2$ under a nitrogen atmosphere. Unless otherwise specified, all reactions were carried out under an argon atmosphere by using standard Schlenk-line techniques. Due to the extreme moisture sensitivity of these compounds, all glassware was pretreated with the commercially available reagent Glassclad.

B. Physical Measurements

The magnetic measurements were performed on polycrystalline samples of the compounds sealed in plastic bags in an inert atmosphere with a SQUID susceptometer (Quantum Design, MPMS-XL-5) in the temperature range 2–300 K at applied magnetic fields ranging from −5 to 5 T. The diamagnetic contributions of the samples were corrected using Pascal's constants.

C. Syntheses

(i) Preparation of $Fe_4Cl_8(THF)_6$, (1)

An amount of $FeCl_2$ (1.00 g, 7.89 mmol) was dissolved in 40 mL of THF and refluxed for 12 h. An off-white precipitate was obtained along with a pale brown solution, which was removed via cannula techniques. The solid was washed with THF, followed by Et_2O, and dried *in vacuo* to give an off-white compound, $Fe_4Cl_8(THF)_6$ (yield: 1.44 g, 78% based on $FeCl_2$). *Anal.* Calcd for $Fe_4Cl_8O_6C_{24}H_{48}$: C, 30.68%; H, 5.15%. Found: C, 30.28%; H, 4.98%. IR (Nujol, cm^{-1}): 1299 (w), 1249 (w), 1180 (w), 1025 (vs), 919 (ms), 874 (vs/br), 674 (w); ν(FeCl), 335 (s), 294 (m), 254 (s).

Single crystals. A saturated solution of $Fe_4Cl_8(THF)_6$ in 20 mL of acetone/0.5 mL of methanol was carefully layered with 2 mL of a buffer solution (acetone/methanol 40:1 v/v) and 10 mL of hexanes in a Schlenk tube. The solution was allowed to stand undisturbed, and within three days a small crop of needle crystals was obtained.

(ii) Preparation of $\{Mn_4Cl_8(THF)_6(Mn(THF)_2Cl_2\}_\infty$, (2)

Bulk preparation. A quantity of $MnCl_2$ (0.500 g, 3.97 mmol) was dissolved in 30 mL of THF in a three-necked Schlenk flask and refluxed for 24 h. The resulting off-white precipitate was collected by filtration, washed with THF followed by Et_2O, and dried *in vacuo* to give a white solid; yield, 0.76 g (82% based on $MnCl_2$). *Anal.* Calcd for $Mn_5Cl_{10}O_8C_{24}H_{64}$: C, 31.90%; H, 5.30%; Cl, 29.40%. Found: C, 30.83%; H, 5.20%; Cl, 29.83%. mid-IR (Nujol, cm^{-1}): 1369 (w), 1345 (vw), 1261 (w), 1172 (vw), 1035 (s, br), 918 (mw), 885 (m,br), 799 (vw), 675. Far-IR (CsI, Nujol, cm^{-1}) ν(Mn–Cl) = 361 (br).

Single-crystal growth. A saturated solution of 100 mg of the product dissolved in 20 mL of acetone/0.5 mL of methanol was carefully layered with 2 mL of a buffer solution (acetone/methanol 40:1 v/v) followed by 10 mL of hexanes in a Schlenk tube. The solution was allowed to stand undisturbed, and after three days a small quantity of needle crystals was obtained. IR (CsI, Nujol, cm^{-1}) ν(Mn–Cl) = 366 (br).

D. X-Ray Crystallography

Crystallographic data for compounds **1** and **2** were collected on a Rigaku AFC6S four-circle diffractometer

and a Bruker (Siemens) SMART 1K CCD platform diffractometer respectively.

(i) $Fe_4Cl_8(THF)_6$ (1)

Although X-ray structures of this compound have been reported by two independent groups who obtained them from different routes (9), a single crystal from our new synthetic method was subjected to crystallographic analysis in order to be certain of the product's identity. The crystal parameters and refinement data are summarized in Table 1. Since this is not a new structure, details of the X-ray structure have been relegated to the supplementary materials section.

(ii) $[Mn_5Cl_{10}(THF)_8]_\infty$ (2)

A colorless, rod-like crystal of approximate dimensions $0.60 \times 0.29 \times 0.29$ mm^3 was mounted on the tip of a glass fiber with Dow Corning silicone grease. Indexing and refinement of 35 reflections from a total of 60 frames with an exposure time of 10 s/frame gave unit cell parameters for a triclinic unit cell. A hemisphere of data with 1321 frames was collected with a scan width of 0.3° in ω and an exposure time of 30 s/frame. Indexing and refinement of 93 strong reflections ($I/\sigma > 10$) generated a precise cell for data integration, which led to 7054 reflections in the range of $-11 \le h \le 7$, $-13 \le k \le 13$, $-15 \le l \le 14$ with a maximum 2θ angle of 52.7°. The final cell was obtained from the refinement of the XYZ centroids of 5400 reflections with $I/\sigma > 10$. The unit cell parameters are $a = 9.4620(2)$ Å, $b = 11.13870(2)$ Å, $c = 12.4763(2)$ Å, $\alpha = 75.2850(10)°$, $\beta = 76.3050(10)°$, $\gamma = 79.6870(10)°$, and $V = 1225.72(3)$ Å^3. The data were corrected for beam inhomogeneity, crystal decay, and absorption by SADABS (10a), which led to transmission factors ranging from 0.81 to 0.46. Of the 4770 unique reflections used for structure solution and refinement, a total of 3720 reflections are in the category $I > 2\sigma(I)$ and $R_{\text{int}} = 0.0302$.

The positions of the nonhydrogen atoms were located by direct methods and refined by full-matrix least squares on F^2 using the SHELXTL 5.04 package (10b). Two disordered THF molecules were modeled in two positions at occupancies of 0.53/0.47% and 0.59/0.41%. All nonhydrogen atoms were refined anisotropically except the disordered THF groups, which were refined isotropically. Hydrogen atoms were placed in idealized positions. The final R_1 ($I > 2\sigma$) value is 0.054 and the wR_2 value is 0.14. Crystallographic data are summarized in Table 1.

TABLE 1
Crystal Data and Structure Refinement for $[Fe_4Cl_8(THF)_6]$, (1) and $\{Mn_4Cl_8(THF)_6(Mn(THF)_2Cl_2\}_8$, (2)

Identification code	(1)	(2)
Empirical formula	$C_{24}H_{48}\ Cl_8Fe_4O_6$	$C_{32}H_{64}Cl_{10}Mn_5O_8$
Formula wt.	939.67	1206.03
Temp (K)	173(2)	133(2)
Wavelength	0.71073 Å	0.71073 Å
Space group	P − 1	P − 1
a (Å)	10.449(3)	9.4620(2)
b (Å)	10.893(4)	11.1387(1)
c (Å)	9.939(3)	12.4763(2)
α (°)	111.75(2)	75.285(1)
β (°)	97.42(3)	76.305(1)
γ (°)	63.47(2)	79.687(1)
V (Å^3)	939(1)	1225.72(3)
Z	1	1
$d_{\text{calc (g/cm}^3)}$	1.704	1.634
μ (cm^{-1})	21.25	18.4
	$^bR = 0.033$, $R_w = 0.047$ [F, $F > 3\sigma(F)$]	$^aR_1 = 0.054$, $wR_2 = 0.14$ [F^2, $I > 2\sigma(I)$]

$^aR_1 = \sum||F_o| - |F_c||/\sum|F_o|$, $wR_2 = \{\sum[w(F_o^2 - F_c^2)^2]/\sum[w(F_o^2)^2]\}^{1/2}$, $w = 1/[\sigma^2(F_o^2) + (aP)^2 + bP]$.

$^bR = \sum||F_o| - |F_c||/\sum|F_o|$, $R_w = \{\sum[w(|F_o| - |F_c|)^2]/\sum[w|F_o|^4]\}^{1/2}$, $w = 1/\sigma^2(|F_o|)$.

DISCUSSION

A. Synthetic Considerations

The cluster $Fe_4Cl_8(THF)_6$ was first reported by Bulychev *et al.*, who unexpectedly obtained the product from the reaction of $FeCl_3$ and Cp_2ReH in THF (9a). The same cluster was later prepared by Cotton and co-workers from a comproportionation reaction of $FeCl_3$ with metallic Fe in refluxing THF (9b). We have found that the most convenient method for obtaining pure $Fe_4Cl_8(THF)_6$ in high yields is to reflux a suspension of anhydrous $FeCl_2$ in THF. An X-ray study on a single crystal obtained from this synthetic procedure confirmed the identity of the compound. As found in the earlier studies, the compound is composed of tetranuclear Fe clusters whose geometry consists of two octahedral and two pseudo five-coordinate Fe centers. Selected bond distances and bond angles and an ORTEP of $Fe_4Cl_8(THF)_6$ from our new data set are presented in Table 2 and Fig. 1, respectively.

Attempts to synthesize $Mn_4Cl_8(THF)_6$ from a procedure similar to that used to prepare $Co_4Cl_8(THF)_6$ and $Fe_4Cl_8(THF)_6$, namely by refluxing $MnCl_2$ in THF, yielded a white material that is a polymeric version of the tetranuclear cluster as described in the following section.

B. X-Ray Structural Results and Discussion

Structure of $\{Mn_4Cl_8(THF)_6(Mn(THF)_2Cl_2\}_\infty$ (2)

An ORTEP diagram of a portion of the chain in **2** is provided in Fig. 2 and selected bond distances and angles are provided in Table 2. A packing diagram in the *bc* plane is depicted in Fig. 3. Unlike the related clusters

TABLE 2
Selected Interatomic Distances (Å) and Bond Angles (°) for $[Fe_4Cl_8(THF)_6]$, (1) and $\{Mn_4Cl_8(THF)_6(Mn(THF)_2Cl_2\}_8$, (2)

		Bond distances			
A	B	A–B (Å)	A	B	A–B (Å)
Fe1	Fe1*	6.209(1)	Fe1	O1	2.136(2)
Fe2	Fe2*	3.615(1)	Fe2	Cl1	2.459(1)
Fe1	Cl1	2.354(1)	Fe2	O2	2.139(2)
Fe1	Cl2	2.261(1)	Fe2	O3	2.111(2)
Fe1	Cl3	2.371(1)	Fe2	Cl4	2.159(2)
Fe1	Cl4	2.682(1)	Fe2	Cl4*	2.502(1)

			Bond angles				
A	B	C	A–B–C (°)	A	B	C	A–B–C (°)
Cl1	Fe1	Cl2	125.90(5)	Cl1	Fe2	Cl4	87.07(4)
Cl1	Fe1	Cl3	110.21(4)	Cl1	Fe2	O2	88.76(8)
Cl2	Fe1	Cl3	123.22(4)	Cl1	Fe2	O3	88.87(7)
O1	Fe1	Cl1	89.34(8)	Cl1	Fe2	Cl3*	176.80(3)
O1	Fe1	Cl2	94.02(8)	Fe2	Cl4	Fe2*	96.28(4)
O1	Fe1	Cl3	92.38(7)	Cl4	Fe2	Cl4*	83.72(4)
Fe1	Cl1	Fe2	97.98(5)				

		Bond distances			
A	B	A–B (Å)	A	B	A–B (Å)
Mn1	Mn1A	3.751(1)	Mn2	Mn2A	6.495(1)
Mn1	Mn2	3.763(1)	Mn2	Mn1A	3.738(1)
Mn1	Cl1	2.454(1)	Mn2	Cl1	2.550(1)
Mn1	Cl2	2.601(1)	Mn2	Cl2	2.602(1)
Mn1	Cl5A	2.494(1)	Mn2	Cl3	2.526(1)
Mn1	Cl2A	2.593(1)	Mn2	Cl5	2.559(1)
Mn1	O1	2.238(3)	Mn2	O3	2.227(8)
Mn1	O2	2.195(6)	Mn2	Cl4	2.532(1)
Mn2	Mn3	3.685(1)	Mn3	Cl4	2.551(1)
Mn3	Cl3	2.524(1)	Mn3	O4	2.218(3)

			Bond angles				
A	B	C	A–B–C (°)	A	B	C	A–B–C (°)
Cl1	Mn1	Cl2	86.02(3)	Cl1	Mn2	Cl5	87.07(4)
Cl1	Mn1	Cl5A	177.66(4)	Cl1	Mn2	Cl2	88.76(8)
Cl2	Mn1	Cl5A	93.00(3)	Cl1	Mn2	Cl3	88.87(7)
Cl2	Mn1	Cl2A	87.52(3)	Cl1	Mn2	O3	176.80(3)
Cl1	Mn1	O1	93.33(7)	Cl2	Mn2	Cl5	96.28(4)
Cl1	Mn1	O2	92.1(2)	Cl2	Mn2	Cl4	83.72(4)
Cl2	Mn1	O1	90.41(7)	Mn1	Cl1	Mn2	96.47(3)
Cl2	Mn1	O2	177.9(3)	Mn1	Cl2	Mn2	96.46(3)
Cl2A	Mn1	O1	175.25(7)	Mn2	Cl2	Mn1A	92.04(3)
O1	Mn1	O2	88.8(2)	Mn1	Cl2	Mn1A	92.48(3)
Cl4	Mn2	Cl3	86.68(3)	Cl3	Mn3	Cl4	86.31(3)
Cl4	Mn2	O3	97.8(3)	Cl3	Mn3	Cl4B	93.69(3)
Cl4	Mn2	Cl1	174.79(3)	Cl3	Mn3	O4	89.92(7)

$Co_4Cl_8(THF)_6$ and $Fe_4Cl_8(THF)_6$, which exist as discrete molecular species, the Mn(II) derivative crystallizes as a one-dimensional polymeric chain. The structure of $\{Mn_5Cl_{10}(THF)_8\}_\infty$ is best described as consisting of alternating $Mn_4Cl_8(THF)_6$ and $MnCl_2(THF)_2$ repeat units linked by chloride bridges. This situation leads to three

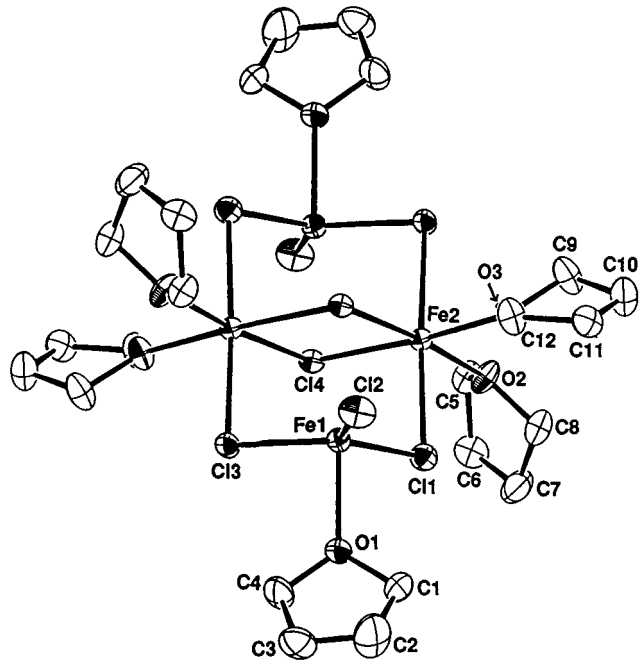

FIG. 1. Thermal ellipsoid plot of $Fe_4Cl_8(THF)_6$.

different types of Mn environments, namely those found in *trans*-$MnCl_4(THF)_2$, $MnCl_5(THF)$, and *cis*-$MnCl_4(THF)_2$ fragments. The presence of the mononuclear "$MnCl_2(THF)_2$" bridge allows for all the metal ions to be six-coordinate, as opposed to the Fe and Co clusters in which there are two five-coordinate and two six-coordinate metal centers. This is not unexpected, given that the larger Mn(II) ion is much less likely to form five-coordinate structures in the absence of steric hindrance than is Co(II) or Fe(II).

A comparison of the metrical parameters of the tetranuclear unit in the Fe, Mn, and Co compounds was made, and

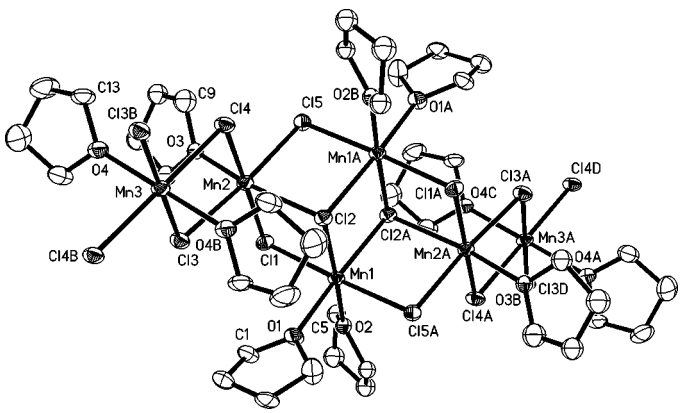

FIG. 2. Thermal ellipsoid plot of $\{Mn_4Cl_8(THF)_6(Mn(THF)_2Cl_2\}_\infty$ with labels.

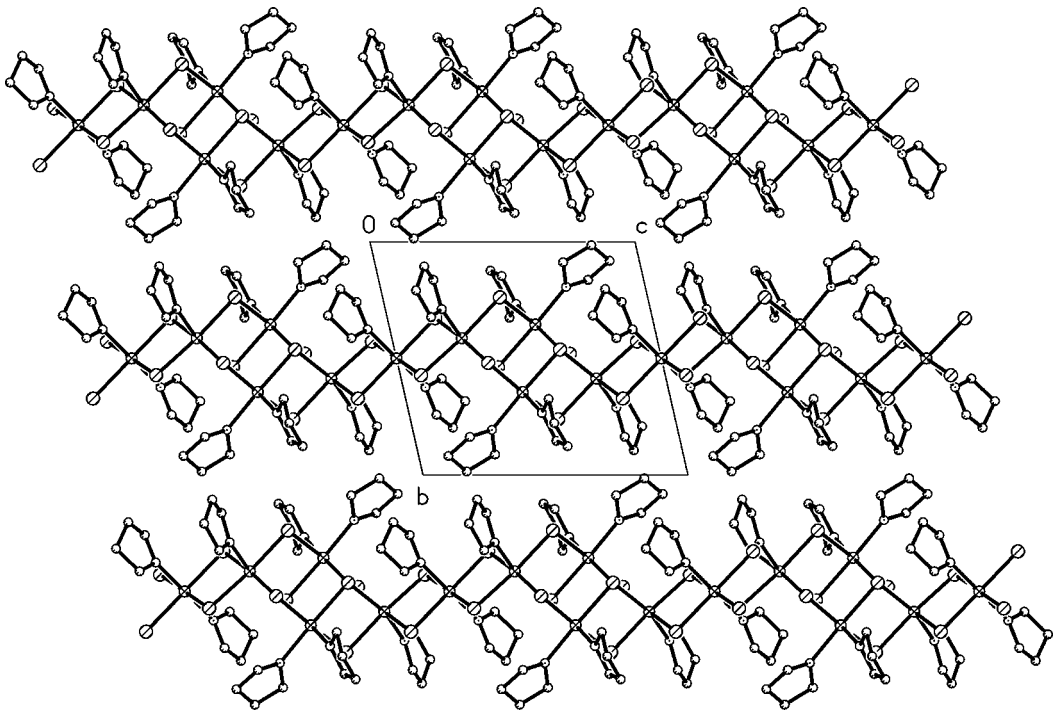

FIG. 3. Packing view of $\{Mn_4Cl_8(THF)_6(Mn(THF)_2Cl_2\}_\infty$ in the *bc* plane.

the results are summarized in Table 3. The parameters for $Co_4Cl_8(THF)_6$ were taken from Ref. (3). For the sake of clarity, models of the discrete Fe and Co clusters and of the tetranuclear unit in the Mn case are depicted in Fig. 4 with a uniform labeling scheme to use for quoting distances. The terminal chloride ligands on the five coordinate metal atoms in the Fe and Co molecules become μ_2-Cl bridges between $\{Mn_4Cl_8(THF)_6\}$ and $MnCl_2(THF)_2$ units in the new compound. This can be easily seen in the schematic diagrams provided in Fig. 5. The μ_2-Cl and μ_3-Cl bridging interactions within the tetranuclear units exhibit similar geometries in all three compounds. The Mn–(μ_2-Cl) distances range from 2.494(1) to 2.558(1) Å and the Mn–(μ_3-Cl) distances are all ~2.60 Å. The other two compounds exhibit M–(μ_2-Cl) values of 2.354(1)–2.459(1) Å for $M = Fe$ and 2.285(2)–2.465(2) Å for $M = Co$. For the M–(μ_3-Cl) interactions, the distances range from 2.519(2) to 2.682(1) Å for $M = Fe$ and 2.435(2)–2.884(3) Å for $M = Co$. Clearly, $\{Mn_4Cl_8(THF)_6(Mn(THF)_2Cl_2\}_\infty$ is much more symmetrical than the other two compounds, with its more narrow range of observed bond lengths. The angle $M1$–Cl(μ_3)–$M1$*, which defines an edge between the two central octahedral M(II) centers, is more acute in all three compounds (approx. 92°–96°) than the outer $M1$–Cl(μ_2)–$M2$ angles (approx. 96°–102°). As a consequence of this, the $M1$–$M2$ distances that define the edges of the cluster are longer than the short body diagonal $M1$–$M1$* with the exception of the Fe derivative. The range for Mn–Mn is 3.738(1) to 3.763(1) Å, the Co–Co range is 3.630(2)–3.686(2) Å, and the Fe–Fe range is 3.615(2)–3.739(2) Å.

TABLE 3
Selected Interatomic Distances (Å) and Bond Angles (°) for $[Fe_4Cl_8(THF)_6]$, (1), $\{Mn_4Cl_8(THF)_6(Mn(THF)_2Cl_2\}_\infty$, (2), and $[Co_4Cl_8(THF)_6]$, (3)

	Fe(1)	Mn(2)	Co(3)
$M1 \ldots M1$*	3.739(1)	3.738(1)	3.630(2)
$M1 \ldots M2$	3.615(1)	3.751(1)	3.646(2)
$M1$* $\ldots M2$	3.633(1)	3.763(1)	3.686(2)
$M2 \ldots M2$*	6.209(1)	6.495(1)	6.370(2)
$M1$–Cl(μ_3)	2.519(2)	2.601(1)	2.435(2)
			2.450(2)
$M2$–Cl(μ_3)	2.682(1)	2.602(1)	2.884(3)
$M1$–Cl1(μ_2)	2.459(1)	2.494(1)	2.465(2)
$M2$–Cl1(μ_2)	2.354(1)	2.550(1)	2.285(2)
$M2$–Cl3(μ_2)	2.371(1)	2.558(1)	2.285(2)
$M2$–Cl4	2.261(1) *t*	2.525(1) *b*	2.216(2) *t*
Cl(μ_3)–$M1$–Cl(μ_3)*	83.72(4)	87.52(3)	84.0(1)
Cl1(μ_2)–$M2$–Cl3(μ_2)	110.21(4)	91.40(3)	113.0(1)
$M1$–Cl1(μ_2)–$M2$	98.02(5)	96.46(3)	101.7(1)
$M1$–Cl(μ_3)–$M1$*	96.28(4)	92.48(3)	96.0(1)

Note. The labeling scheme for this table is found in Fig. 4. (*b* = bridging, *t* = terminal.

C. Magnetic Studies

The magnetic properties of the tetranuclear clusters of Fe and Co and those of the Mn chain were probed

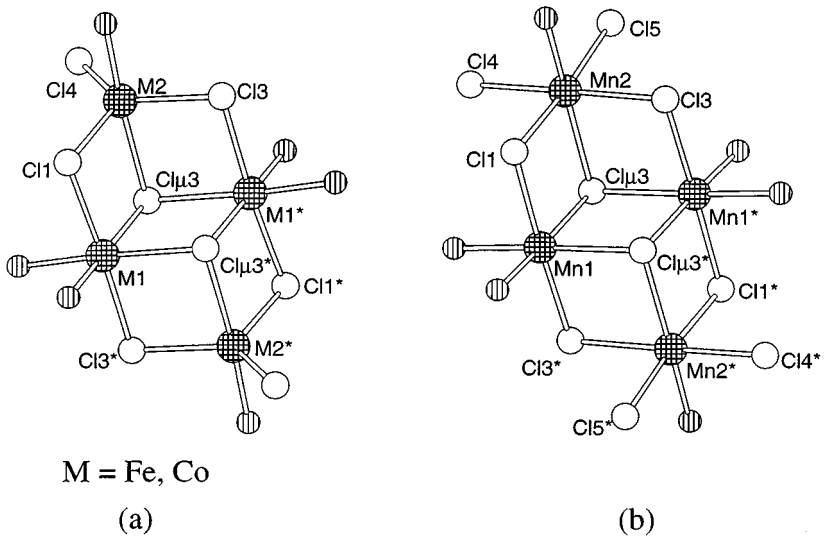

FIG. 4. Views of the cluster cores for (a) $M_4Cl_8(THF)_6$ (M = Fe, Co) and (b) $\{Mn_4Cl_8(THF)_6(Mn(THF)_2Cl_2\}_\infty$ with atom labels used as in Table 3.

in detail, and the results are presented in the following section.

(i) Magnetic Behavior of $Fe_4Cl_8(THF)_6$

Magnetic measurements of $Fe_4Cl_8(THF)_6$ in the temperature range of 79–294 K were reported by Bulychev *et al.*, with the results suggesting an overall ferromagnetically coupled Fe(II) tetramer (9a). We undertook a more thorough investigation of the magnetism of this interesting cluster, with particular emphasis on the low-temperature range and on the field dependence studies. Our goal was to establish the true magnetic ground state of the cluster, if possible, and to fully understand the cooperative effect observed at low temperatures.

The χT versus T plot shows a value of 20 emu.K.mol^{-1} at room temperature that increases with cooling to a maximum of $\sim$51 emu.K.mol^{-1} at 25 K followed by a sharp decrease to a value close to 0 at very low temperatures (Fig. 6). The value of χT at room temperature is significantly higher than what one would expect for four independent spins of $S = 2$ (12 emu.K.mol^{-1}). This is due to the presence of an orbital contribution to the magnetic moment, as high-spin octahedral Fe(II) possesses an orbitally

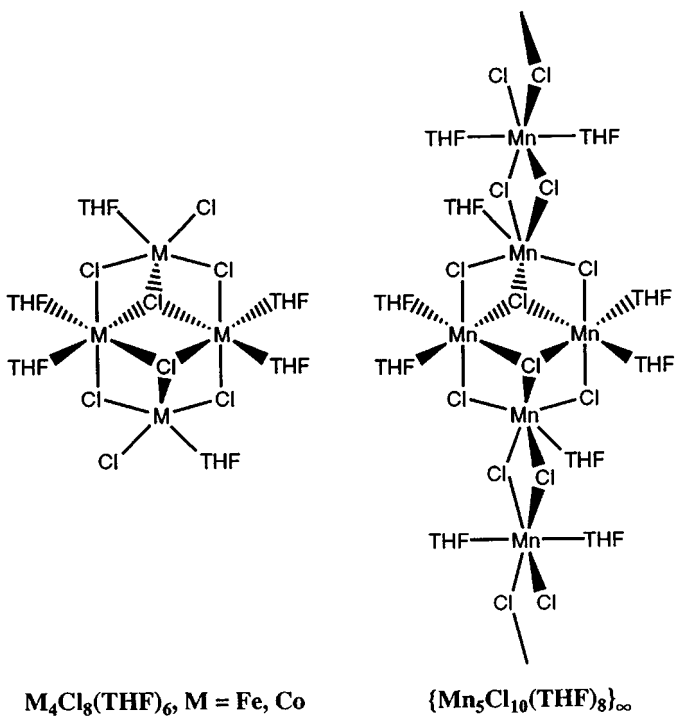

FIG. 5. Schematic diagrams of the discrete clusters $M_4Cl_8(THF)_6$ (M = Fe, Co) and the chain $\{Mn_4Cl_8(THF)_6(Mn(THF)_2Cl_2\}_\infty$.

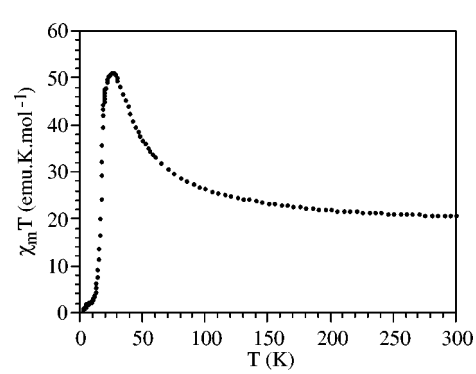

FIG. 6. Thermal variation of $\chi_m T$ for $Fe_4Cl_8(THF)_6$ at an applied field of 0.01 T.

degenerate ground state, $^5T_2$. The continuous increase of χT with cooling indicates that the four Fe(II) centers in the rhombic cluster are ferromagnetically coupled. The sharp decrease of χT at lower temperatures may be a consequence of antiferromagnetic intercluster interactions in the 3D lattice, which favor a long-range antiferromagnetic ordering.

To analyze the magnetic properties of this compound the data were divided into two parts: (1) the high-temperature paramagnetic region where short-range effects originating from the magnetic exchange interactions within the cluster can be observed, and (2) the low-temperature region where cooperative properties are observed. By examining the high-temperature paramagnetic region one can extract quantitative information about the Fe(II)′–Fe(II) exchange interactions in the cluster (Fig. 7). In view of the orbital degeneracy of Fe(II), an anisotropic exchange model has been used to treat the data (note that the model is equivalent to an isotropic exchange model supplemented by a large single-ion anisotropy). The cluster has two different types of exchange pathways, *viz.*, J for the pairwise Fe–(μ–Cl)–Fe interactions along the edges of the cluster and J' for the Fe_2–$(\mu\text{–Cl})_2$ interactions (see Scheme 2). Each has been assumed to exhibit an axial anisotropy with parallel (z) and perpendicular (xy) components. The same type of anisotropy has been assumed for the g tensors of the individual ions. This anisotropic exchange Hamiltonian can be written as

$$\begin{aligned} H = &-2J_z(S_{z1}S_{z3} + S_{z1}S_{z4} + S_{z2}S_{z3} + S_{z2}S_{z4}) - 2J_{z'}S_{z1}S_{z2} \\ &- 2J_{xy}(S_{x1}S_{x3} + S_{x1}S_{x4} + S_{x2}S_{x3} + S_{x2}S_{x4} \\ &+ S_{y1}S_{y3} + S_{y1}S_{y4} + S_{y2}S_{y3} + S_{y2}S_{y4}) \\ &- 2J_{xy'}\,(S_{x1}S_{x2} + S_{y1}S_{y2}) \end{aligned} \qquad [1]$$

Including the g parameters, this model contains six parameters (four J and two g components). As has been pointed out in previous papers, magnetic susceptibility can only provide reliable information about the sign of the exchange interactions, but it is not very sensitive to the magnitude of exchange anisotropy (11). Due to this situation, the number of independent parameters has been reduced to 5 by assuming the same anisotropy, R, for the two kinds of exchange parameters: $R = J_{xy}/J_z = J'_{xy}/J'_z$. The eigenvalues of the spin

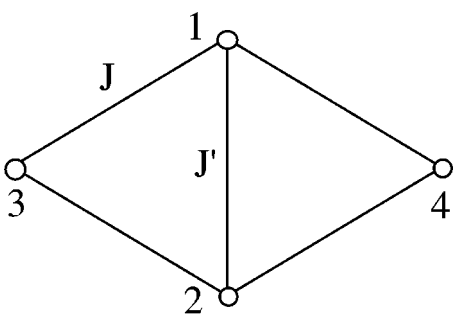

SCHEME 2. Model of the exchange interactions between the four metal centers in the $M_4Cl_8(THF)_6$ clusters.

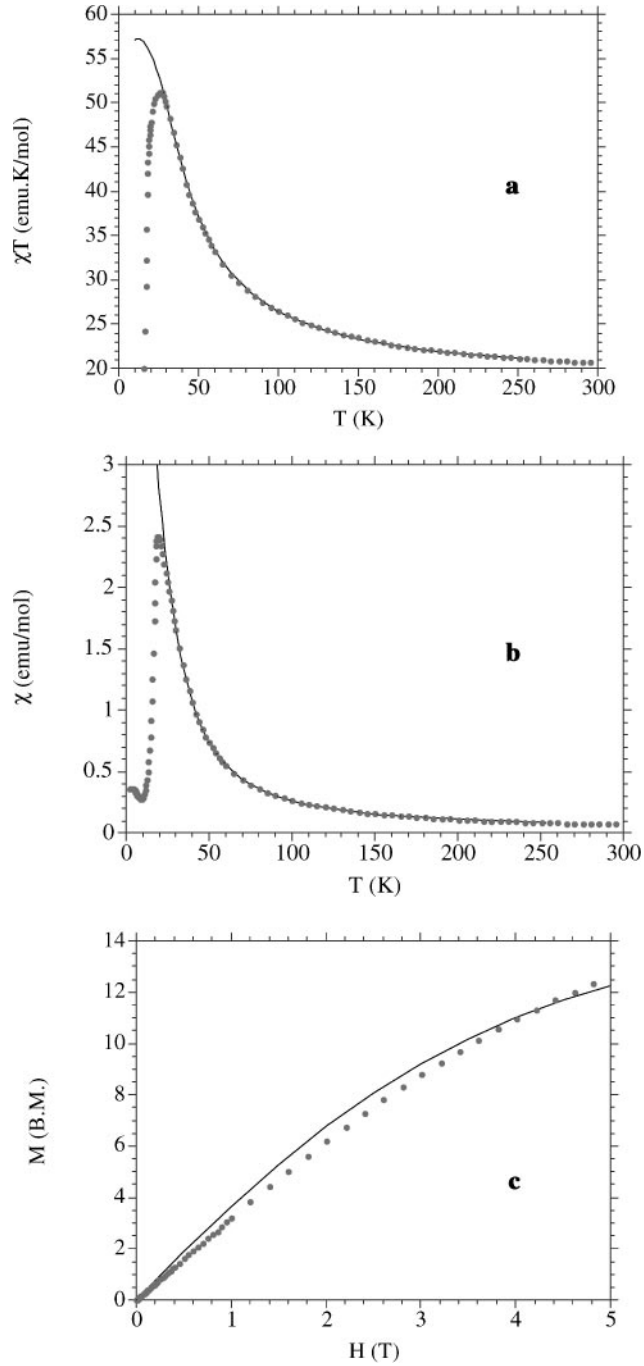

FIG. 7. Magnetic properties of $Fe_4Cl_8(THF)_6$: (a) high-temperature range of the thermal variation of the $\chi_m T$ product (filled circles) and best fit to the experimental data obtained using Eq. [1] (solid line), (b) thermal variation of χ_m (filled circles) and best fit (solid line), and (c) experimental magnetization curve at 30 K (filled circles) and simulation using the $\chi_m T$ product fit parameters.

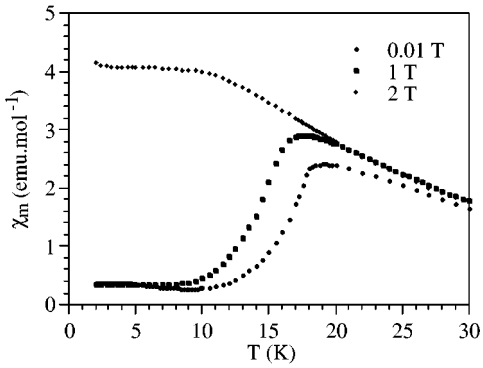

FIG. 8. Thermal variation of the molar susceptibility for $Fe_4Cl_8(THF)_6$ at different applied fields.

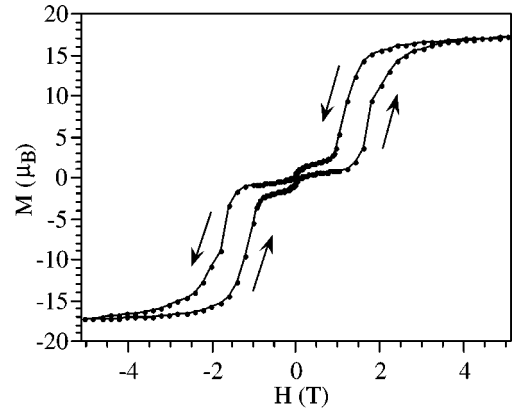

FIG. 10. Hysteresis loop for $Fe_4Cl_8(THF)_6$ at 2 K.

Hamiltonian in Eq. [1] have been calculated by using the computer approach based on the irreducible tensor operator techniques developed by Coronado and co-workers (12). This model reproduces, in a satisfactory fashion, the magnetic susceptibility data above 30 K. The following set of parameters are obtained: $J_z = 4.7\ \text{cm}^{-1}$, $J'_z = 0.5\ \text{cm}^{-1}$, $R = 0.45$, $g_z = 2.6$, and $g_{xy} = 2.4$. These parameters also reproduce the magnetization data at 30 K (Fig. 7c). From this analysis, one can assess that the coupling within the cluster is ferromagnetic and larger for the edges of the cluster. The presence of an exchange anisotropy is required to reproduce the data.

Now let us turn to the low-temperature region where it can be seen that the susceptibility is strongly dependent on the external magnetic field (Fig. 8). Thus, when the magnetic field is 0.01 T, χ presents a maximum at $\sim$20 K. At higher magnetic fields this maximum is displaced toward lower temperatures (17 K at 1 T) until at 2 T it disappears and the susceptibility saturates. The antiferromagnetic interactions are canceled when the magnetic field reaches a critical value sufficient to stabilize a phase with a net magnetic moment, behavior that is characteristic of metamagnets. In order to confirm the metamagnetic behavior, and to accurately determine the critical field (H_c) at which the antiferromagnetic interactions are canceled, isothermal magnetization measurements were performed at $T < 20$ K. These data reveal an abrupt increase in the magnetic moment at $\sim$1.4 T at 5 and 10 K; the increase occurs at 1.8 T at 2 K (Fig. 9). This step in the magnetic moment indicates a transition from the antiferromagnetic phase at low fields, where the magnetic moment is essentially zero, to a field-induced ferromagnetic phases at high fields, where the magnetic moment reaches the value expected for a ferromagnetically coupled Fe_4 cluster. Within the antiferromagnetic phase, magnetic hysteresis is also observed at 2 K (Fig. 10).

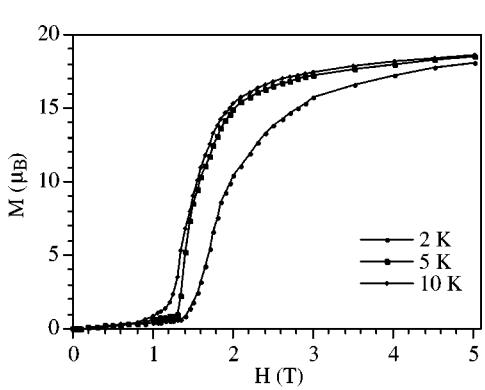

FIG. 9. Magnetization curves for $Fe_4Cl_8(THF)_6$ at different temperatures.

(ii) Magnetic Behavior of $Co_4Cl_8(THF)_6$

The χT vs T plot shows a r.t. value of 10.5 emu.K.mol^{-1} (Fig. 11a) that decreases with cooling to a minimum of 4 emu.K.mol^{-1} at $\sim$12 K (inset in Fig. 11a) followed by a smooth increase at lower T and a very sharp increase at $\sim$3.5 K (Fig. 11b). The room temperature value of χT is within the range corresponding to four high-spin, octahedral Co(II) ions. Since the magnetic cluster contains two different coordination modes for Co (hexa- and tetracoordinate), one would expect different local magnetic moments for these two sites. It is also expected that the spin-orbit coupling of octahedral Co(II) contributes to the decrease of the χT product. Still, this decrease is too prominent to be attributed solely to this effect, and, therefore, the presence of antiferromagnetic exchange interactions within the cluster must be considered as well. In order to obtain information on the exchange interactions within the Co_4 cluster, an anisotropic exchange model similar to that used for the Fe_4 cluster has been used to fit the susceptibility data. To explain the magnetic interactions in Co(II) clusters, the most popular approximation is to assume that octahedral Co(II) can be well described below 30–50 K as an anisotropic

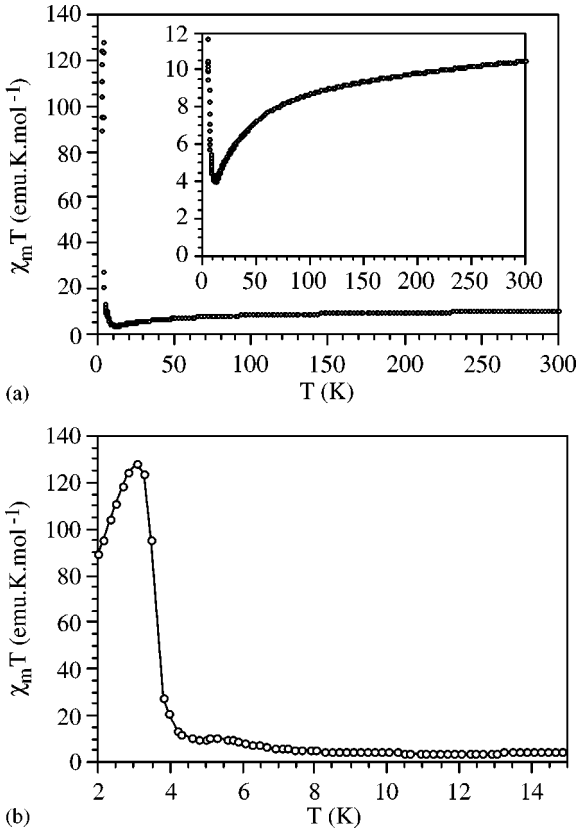

FIG. 11. (a) Thermal variation of the $\chi_m T$ product for $Co_4Cl_8(THF)_6$ at an applied field of 0.01 T. (Inset) The high-temperature region showing the minimum at $\sim$12 K. (b) Variation of the $\chi_m T$ product for $Co_4Cl_8(THF)_6$ at low temperature.

Kramers doublet, i.e., by an effective anisotropic spin $S = \frac{1}{2}$. An isotropic spin $S = \frac{3}{2}$ has been assumed for tetracoordinated Co(II). This type of approach provides information on the exchange interactions when the interactions are weak compared to the thermal energy in this region of temperature. This occurs for J values smaller than 8–10 cm^{-1}. When the exchange interactions are stronger, however, the range of temperatures that can be used in the analysis is insufficient to extract this information. Our cluster is in this limit. Furthermore, our system is complicated by the presence of strong intercluster interactions, as noted above for the Fe_4 cluster, that affect the susceptibility data at temperatures near and below the minimum in χT (placed at 12 K). With these limitations in mind, we have attempted to identify the range of parameters that are able to reproduce the characteristic minimum in χT. The results are indicative of an antiferromagnetic exchange interaction J_z for the sides of the cluster Co–(μ–Cl)–Co on the order of 5–10 cm^{-1}, as well as a weaker interaction along the short diagonal of the cluster for Co–$(\mu\text{–Cl})_2$–Co.

The sharp increase in the χT product at low temperatures suggests the presence of a transition to an ordered state at

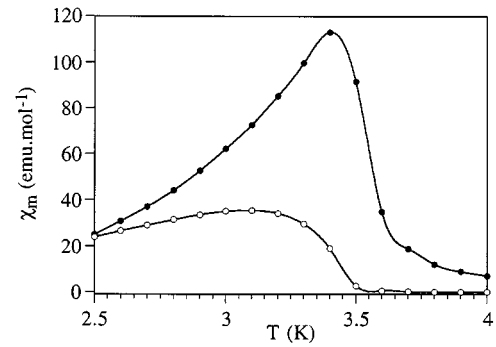

FIG. 12. a.c. susceptibility at a frequency of 332 Hz with an oscillating field of 3.95 G for $Co_4Cl_8(THF)_6$. Filled circles, in-phase signal; open circles, out-of-phase signal.

$\sim$3.5 K. To elucidate the nature of this magnetic transition, a.c. and zero-field-cooled (ZFC) measurements were performed. The a.c. susceptibility shows a peak in both the in-phase and out-of-phase signals at $\sim$3.5 K (Fig. 12). This confirms the existence of a long-range magnetic ordering in which there is a net magnetic moment. No frequency dependence is observed, which rules out the possibility of superparamagnetism or glassy behavior.

The existence of an ordered state below 3.5 K that presents a remnant magnetization is also observed in the ZFC and FC measurements that show a peak at 3.5 K when the sample is cooled in zero field and then warmed at an applied field of 1 G (curve 1 in Fig. 13) (1 T = 10^4 G). This maximum is not observed when the sample is cooled in an applied field of 1 G (curve 2 in Fig. 13). Finally, after removal of the magnetic field, the sample shows a remnant magnetization that vanishes at $\sim$3.5 K (curve 3 in Fig. 13).

The aforementioned data suggest the possibility of several ordered phases, including ferromagnetic, ferrimagnetic, and canted antiferromagnetic. Magnetization measurements provide useful information in clarifying which of these cases

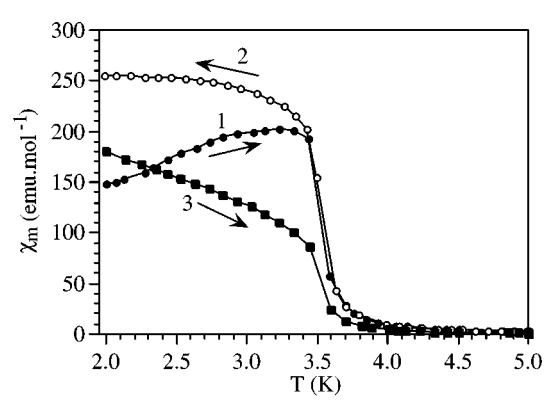

FIG. 13. Zero-field cooled susceptibility data for $Co_4Cl_8(THF)_6$. Curve 1, warming at an applied field of 1 G after zero-field cooling; curve 2, cooling at 1 G; and curve 3, remnant susceptibility in warming at 0 G.

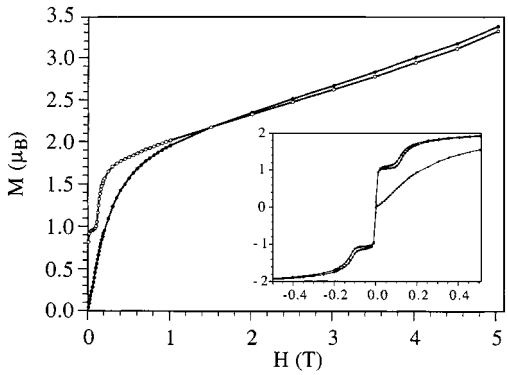

FIG. 14. Magnetization curves for $Co_4Cl_8(THF)_6$ at 2 K (open ircles) and 5 K (filled circles). (Inset) Low-field region of the hysteresis loop at 2 K (open circles) compared with the 5 K curve (filled circles)

is most likely. At 2 K, the magnetization shows an abrupt increase of the magnetic moment at low fields reaching a value of approximately 1 μ_B at 0.01 T followed by a plateau and a second increase at $\sim$0.12 T (inset in Fig. 14). The increases show hysteresis loops with coercivities of $\sim$0.004 and 0.015 T, respectively. At higher fields the magnetic moment increases steadily with magnetic field to reach a value of $\sim$3.5 μ_B at 5 T (Fig. 14). This value is lower than that expected for four parallel Co (II) magnetic moments ($\sim$10–12 B.M.) and confirms the antiferromagnetic nature of the Co(II)–Co(II) interactions within the cluster.

What is quite remarkable in this compound is that a field of only a few gauss is sufficient to produce a sharp increase in the magnetic moment and to reach the first step. As a consequence, this sample is extremely sensitive to the sign of the applied magnetic field, so a reversal of this sign leads to a rapid inversion of the magnetic moment of the sample. In this sense the sample behaves as a very soft magnet. At 5 K the magnetic moment shows an abrupt increase until aprox. 1 T without any step and then follows the same behavior as at 2 K (Fig. 14).

Clearly the aforementioned behavior is more complex than that of a ferromagnet or a ferrimagnet. One possible explanation for the observed behavior is to describe the compound as a canted metamagnet. In fact, it is possible to have an intermediate ground spin state caused by an incomplete compensatation of the two slightly different magnetic moments associated with the two kinds of Co(II) sites with antiferromagnetic coupling. Spin frustration effects can also contribute to the stabilization of this intermediate spin state. Therefore, at low temperatures each cluster can be described by an anisotropic magnetic moment. One can envisage that in the solid state, that these magnetic moments interact due to antiferromagnetic intercluster interactions to give an antiferromagnetic ordering below T_c. Due to the large spin anisotropy of Co(II), however, these moments are not completely antiparallel but have a canting angle. This

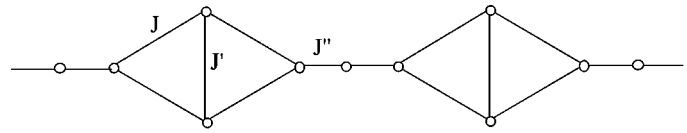

SCHEME 3. Model of the exchange interactions between the Mn centers in $\{Mn_4Cl_8(THF)_6(Mn(THF)_2Cl_2\}_\infty$.

feature accounts for the plateau observed at 1 μ_B at low fields. At fields higher than 0.1 T, the antiparallel canted moments can flop, as in a metamagnet. This accounts for the sharp increase observed in the magnetization and allows for an estimation of a critical field of approx. 0.1 T for this compound.

(iii) Magnetic Behavior of $\{Mn_4Cl_8(THF)_6(Mn(THF)_2Cl_2\}_\infty$

The χT value decreases continuously from $\sim$25 emu.K.mol^{-1} at room temperature to $\sim$10 emu.K.mol^{-1} at 5 K (Fig. 15), which points to an overall antiferromagnetic coupling in the Mn(II) chain. In order to fit the magnetic data, one must invoke a 1-D model involving three different exchange pathways as diagrammed in Scheme 3. This exchange network comprises the two kinds of interactions within the tetranuclear rhombic cluster, namely J and J', and a third interaction, J'', that accounts for the coupling between adjacent clusters in the chain. No exact model is available for this system, therefore an approximation was used in which one assumes a closed finite chain formed by a tetranuclear cluster of $S = \frac{5}{2}$ spins connected to an $S = \frac{5}{2}$ spin. This model closely reproduces the experimental behavior from the following set of parameters: $J = -0.21 \pm 0.01$ cm^{-1}, $J' = 0.0 \pm 0.1$ cm^{-1}, $J'' = -0.20 \pm 0.01$ cm^{-1}, and $g = 2.0$. This simplified model led to the ratio J'/J being smaller than 1.2, which is the necessary condition to ensure an $S = 0$ ground spin state for the cluster. If this condition was not satisfied, an intermediate

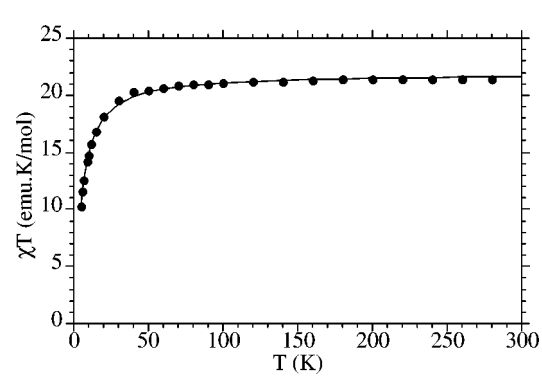

FIG. 15. Thermal variation of the $\chi_m T$ product for the polymeric chain $\{Mn_4Cl_8(THF)_6(Mn(THF)_2Cl_2\}_\infty$ and the best fit obtained from the closed finite chain approach.

ground state for the cluster would result, and the chain would behave as a 1-D ferrimagnet, since the spin of the Mn_4 cluster and the spin of the bridging Mn(II) have different values. Experimentally, one observes antiferromagnetic behavior, which rules out such a possibility.

CONCLUSIONS

The divalent chlorides MCl_2 (M = Fe, Co) react with THF to produce tetranuclear clusters whereas $MnCl_2$ reacts with THF to yield a chain of tetranuclear clusters. The basic intracluster magnetic interactions have been modeled, which sets the stage for a better understanding of more complicated molecular arrays prepared from the cluster building blocks. The presence of ferro- and antiferromagnetic anisotropic interactions within the Fe and Co clusters and significant intercluster interactions gives rise to complex long-range magnetic orderings at low temperatures; these include metamagnetism in the Fe derivative and weak ferromagnetism combined with metamagnetism in the Co derivative.

ACKNOWLEDGMENTS

K.R.D. gratefully acknowledges the National Science Foundation (NSF CHE-9906583) and the Welch Foundation for support of this work and NSF for funding the CCD diffractometer (CHE-9807975) and the SQUID instrumentation (NSF-9974899). This work was supported by the Spanish Ministerio de Ciencia y Tecnología (Grants MAT98-0880 and 1FD97-1765).

REFERENCES

1. (a) F. A. Cotton and R. A. Walton, "Multiple Bonds Between Metal Atoms," 2nd ed. Oxford Univ. Press, New York, 1993; (b) F. A. Cotton, G. Wilkinson, C. A. Murillo, and M. Bochmann, "Advanced Inorganic Chemistry," sixth ed. Wiley, New York, 1999; (c) F. Rogel, J. Zhang, M. W. Payne, and J. D. Corbett, *in* "Centered Cluster Halides for Group-Three and Group-Four Transition Metals" (M. K. Johnson, R. B. King, D. M. Kurtz Jr., C. Kutal, M. L. Norton, and R. A. Scott, Eds., Vol. 226, pp. 367–389. American Chemical Society, Washington, DC, 1990; (d) F. A Cotton, T. Hughbanks, C. E. J. Runyan, and W. A. Wojtczak, *in* "Halide Supported Octahedral Clusters of Zirconium: Structural and Bonding Questions" (M. H. Chisholm, Ed), pp. 1–26. VCH, New York, 1995.
2. (a) C. E. Runyan, Jr. and T. Hughbanks, *J. Am. Chem. Soc.* **116,** 7909 (1994); (b) J. R. Long, A. S. Williamson, and R. H. Holm, *Angew. Chem., Int. Ed. Engl.* **34,** 226 (1995); (c) J. R. Long, L. S. McCarty, and R. H. Holm, *J. Am. Chem. Soc.* **118,** 4603 (1996); (d) Y. Tian and T. Hughbanks, *Inorg. Chem.* **34,** 6250 (1995).
3. (a) F. Rogel and J. D. Corbett, *J. Am. Chem. Soc.* **112,** 8198 (1990); (b) J. M. Tarascon, F. J. DiSalvo, C. H. Chen, P. J. Carroll, M. Walsh, and L. Rupp, *J. Solid State Chem.* **58,** 290 (1985); (c) S. C. Lee and R. H. Holm, *Angew. Chem. Int. Ed. Engl.* **29,** 840 (1990); (d) O. M. Yaghi, M. J. Scott, and R. H. Holm, *Inorg. Chem.* **31,** 4778 (1992).
4. (a) O. Kahn, *Angew. Chem. Int. Ed. Engl.* **24,** 834 (1985); (b) "Proceedings of the Conference on Ferromagnetic and High Spin Molecular Based Materials," J. S. Miller and D. A. Dougherty (Eds.), *Mol. Cryst. Liq. Cryst.* **176** (1994); (c) C. Kollmar and O. Kahn, *Acc. Chem. Res.* **26,** 259 (1993); (d) J. Miller and A. Epstein, *Angew. Chem. Int. Ed. Engl.* **33,** 385 (1994); (e) O. Kahn, D. Gatteschi, J. S. Miller, and F. Palacio (Eds.) "Proceedings of the Conference on Molecular Magnetic Materials," NATO ASI Molecular Magnetic Materials, Vol. E198, Kluwer Academic, Dordrecht, 1991; (f) P. Day, *Science* **261,** 421 (1994); (g) O. Kahn, *Comments Cond. Mater. Phys.* **17,** 39 (1994); (h) D. Gatteschi, A. Caneschi, L. Pardi, and R. Sessoli, *Science* **265,** 1054 (1994); (i) O. Kahn, *Nature* **378,** 667 (1995); (j) O. Kahn, *Act. Chim.* **7,** 62–68; (1996) (k) P. A. Alivisatos, P. F. Barbara, A. W. Castleman, J. Chang, D. A. Dixon, M. L. Klein, G. L. McCLendon, J. S. Miller, M. A. Ratner, P. J. Rossky, S. I. Stupp, and M. E. Thompson, *Adv. Mat.* **10,** 1297 (1998); (l) W. R. Entley and G. S. Girolami, *Science* **268,** 397 (1995); (m) S. Ferlay, T. Mallah, R. Ouahes, P. Veillet, and M. Verdaguer, *Nature* **378,** 701 (1995); (n) M. Verdaguer, *Science* **272,** 698 (1996); (o) O. Sato, Z. Gu, H. Etoh, J. Ichiyanagi, T. Iyoda, A. Fujishima, and K. Hashimoto, *Chem. Lett.* 37 (1997); (p) J. S. Miller and A. J. Epstein, *Chem. Commun.* 1319 (1998); (q) J. Zhang, J. Ensling, V. Ksenofontov, P. Gütlich, A. J. Epstein, and J. S. Miller, *Angew. Chem. Int. Ed.* **37,** 637 (1998); (r) Y. Pei, O. Kahn, K. Nakatani, E. Codjovi, C. Mathonière, and J. Sletten, *J. Am. Chem. Soc.* **113,** 6558 (1991); (s) H. O. Stumpf, Y. Pei, C. Michaut, O. Kahn, J. P. Renard, and L. Ouahab, *Chem. Mater.* **6,** 257 (1994); (t) S. Decurtins, H. W. Schmalle, R. Pellaux, P. Schneuwly, and A. Hauser, *Inorg. Chem.* **35,** 1451 (1996).
5. O. Kahn, "Molecular Magnetism," VCH, Weinheim (1993).
6. (a) S. L. Bartley and K. R. Dunbar, *Angew. Chem. Int. Ed. Eng.* **30,** 1991 (1991); (b) K. R. Dunbar, *Comments Inorg. Chem.* **13,** 313 (1992); (c) K. R. Dunbar and X. Ouyang, "Proceedings of the IV International Conference on Molecule Based Magnets," *Mol. Cryst. Liq. Cryst.* **273,** 21 (1995); (d) K. R. Dunbar and J.-S. Sun, *Mol. Cryst. Liq. Cryst.* **274,** 51 (1995); (e) K. R. Dunbar, *Angew Chem.* **35,** 1659 (1996); (f) K. R. Dunbar *in* "Molecular Magnetism: From Molecular Assemblies to the Devices" (E. Coronado, P. Delhaès, D. Gatteschi, and J. S. Miller, Eds.), NATO ASI Series, Vol. E321, p. 571, Kluwer Academic, Dordrecht, 1996; (g) K. R. Dunbar and R. A. Heintz, *Prog. Inorg. Chem.* **45,** 283 (1996); (h) H. Zhao, R. A. Heintz, R. D. Rogers, and K. R. Dunbar, *J. Am. Chem. Soc.* **118,** 12,844 (1996); (i) K. R. Dunbar and X. Ouyang, *Inorg. Chem.* **35,** 7188 (1996); (j) M. Fourmigué, C. E. Uzelmeier, K. Boubekeur, S. L. Bartley, and K. R. Dunbar, *J. Organomet. Chem.* **529,** 343 (1997); (k) K. R. Dunbar, J. Cowen, H. Zhao, R. A. Heintz, X. Ouyang, and G. Grandinetti, *in* "Supramolecular Engineering of Synthetic Metallic Materials: Conductors and Magnets" (J. Veciana, Ed.) Kluwer, NATO ASI Series, Vol. 518, p. 533, Academic, Dordrecht, 1999; (l) R. A. Heintz, H. Zhao, X. Ouyang, G. Grandinetti, J. Cowen, and K. R. Dunbar, *Inorg. Chem.* **38,** 144 (1999); (m) H. Zhao, R. A. Heintz, X. Ouyang, C. F. Campana, R. D. Rogers, and K. R. Dunbar, *Chem. Mater.* **11,** 736 (1999); (n) J. Cowen, R. Clérac, R. A. Heintz, S. O'Kane, X. Ouyang, H. Zhao, and K. R. Dunbar, *in* "Proceedings of the VIth International Conference on Molecule Based Magnets, September, Seignosse Le Penon, France," *Mol. Cryst. Liq. Cryst.* **335,** 113 (1999); (o) R. Clérac, S. O'Kane, X. Ouyang, H. Zhao, and K. R. Dunbar, *J. Solid State Chem.* **152,** 159 (2000); (p) J. A. Smith, J. R. Galán-Mascarós, R. Clérac, and K. R. Dunbar, *Chem. Commun.* 1077 (2000); (q) H. Miyasaki, C. Campos, and K. R. Dunbar, *Angew. Chem.* **39,** 3831 (2000); (r) H. Miyasaka, C. Campos, J. R. Galán-Mascarós, and K. R. Dunbar, *Inorg. Chem.*, in press (2001); (s) P. S. Szalay, J.-R. Galán-Mascarós, R. Clérac, and K. R. Dunbar, *Synth. Met.*, in press (2001); (t) J. A. Smith, J. R. Galán-Mascarós, R. Clérac, J.-S. Sun, X. Ouyang, and K. R. Dunbar, "Proceedings of the VIIth International Conference on Molecule-Based Magnets, San Antonio, TX, Sept. 16–21," *Polyhedron*, in press (2001); (u) J. R. Galán-Mascarós and K. R. Dunbar, *Chem. Commun.*, in press (2001).
7. (a) K. Awaga, E. Coronado, and M. Drillon, *Mater. Res. Bull.* 52 (2000). (b) E. Coronado, M. Clemente-León, J. R. Galán-Mascarós, C. Gimeenez-Saiz, C. J. Gómez-García, and E. Martínez-Ferrero,

J. Chem. Soc. Dalton Trans. 3955 (2000); (c) E. Coronado, J. R. Galán-Mascarós, and C. J. Gómez-García, *Mol. Synth. Metals* **102,** 1459 (1999); (d) M. Clemente-León, E. Coronado, J. R. Galán-Mascarós, C. Gimeenez-Saiz, C. J. Gómez-García, C. Rovira, and V. N. Lauhkin, *Synth. Metals* **103,** 2339 (1999); (e) M. Clemente-León, E. Coronado, J. R. Galán-Mascarós, and C. J. Gómez-García, *Chem. Commun.* 1727 (1997); (f) E. Coronado, J. R. Galán-Mascarós, C. J. Gómez-García, J. Ensling, and P. Gütlich, *Chem. Eur. J.* **6,** 552 (2000); (g) E. Coronado, J. R. Galán-Mascarós, C. J. Gómez-García, and R. Burriel, *J. Magn. Magn. Mater.* **196–197,** 558 (1999); (h) E. Coronado, J. R. Galán-Mascarós, C. J. Gómez-García, and V. Laukin, *Nature* **408,** 447 (2000); (i) E. Coronado, J. R. Galán-Mascarós, and C. J. Gómez-García, *Mol. Cryst. Liq. Cryst.* **334,** 679 (1999); (j) E. Coronado, J. R. Galán-Mascarós, C. J. Gómez-García, and J. M. Martínez-Agudo, *Adv. Mater.* **11**, 558 (1999); (k) E. Coronado, J. R. Galán-Mascarós, C. J. Gómez-García, and J. M. Martínez-Agudo, *Synth. Metals*, in press.

8. P. Sobota, Z. Olejnik, J. Utko, and T. Lis, *Polyhedron* **12,** 613 (1993).
9. This cluster has been previously reported by reduction of $FeCl_3$: (a) V. K. Bel'skii, V. M. Ishchenko, B. M. Bulychev, A. N. Protskii, G. L. Soloveichik, O. G. Ellert, M. Seifulina, Y. V. Rakitin, and V. M. Novotortsev, *Inorg. Chim. Acta* **96,** 123 (1985); (b) F. A. Cotton, R. L. Luck, and K.-A. Son, *Inorg. Chim. Acta* **179,** 11 (1991).
10. (a) G. M. Sheldrick, "SADABS. Siemens Area Detector Absorption (and other) Corrections," University of Göttingen, Germany, 1998; (b) G. M. Sheldrick, SHELXS-97, Program for Crystal Structure Determination and SHELXL-97, Program for Refinement of Crystal Structures, University of Göttingen, Göttingen, Germany, 1997.
11. N. Casan-Pastor, J. Bas, E. Coronado, G. Puurroy, and L. C. W. Baker, *J. Am. Chem. Soc.* **114,** 10,380 (1992).
12. (a) J. J. Borrás-Almenar, J. M. Clemente-Juan, E. Coronado, and B. S. Tsukerblat, *Inorg. Chem.* **38,** 6081 (1999) (b) J. J. Borrás-Almenar, J. M. Clemente-Juan, E. Coronado, and B. S. Tsukerblat, *J. Comp. Chem.*, submitted.